UNIVERSITY OF LATVIA

FACULTY OF PHYSICS, MATHEMATICS AND OPTOMETRY

Arturs Bundulis

INQUIRY OF THE KERR EFFECT ORIGINS IN ORGANIC MATERIALS: EXPERIMENTAL ASSESSMENT BY Z-SCAN METHOD

SUMMARY OF DOCTORAL THESIS

Submitted for the degree of Doctor of Physics and Astronomy
Subfield: Solid State Physics

Riga, 2020

The work presented in doctoral thesis was carried out in the Institute of Solid State Physics, University of Latvia from 2016 to 2020.

The thesis contains the introduction, three chapters, conclusions, thesis and reference list.

Form of the thesis: dissertation in Physics and Astronomy, Solid State Physics.

Supervisor: Dr. phys. Martins Rutkis, senior researcher at ISSP, University of Latvia.

Reviewers:

1) *Dr. habil. phys.* **Andris Ozols**, Professor, Riga Technical University;
2) *Dr. phys.* **Janis Alnis**, Institute of Atomic Physics and Spectroscopy, University of Latvia;
3) *Prof.* **Jean-Michel Nunzi**, Professor, Queen's University.

The thesis will be defended at the public session of Doctoral Committee of Physics, Astronomy and Mechanics, University of Latvia at 17:00 on December 17, 2020 in the conference hall of the Institute of Solid State Physics of University of Latvia.

The thesis and summary of doctoral thesis is available at the Library of the University of Latvia, Kalpaka bulv. 4.

Chairman of the Doctoral Committee *Dr. habil. phys.* **Uldis Rogulis**

Secretary of the Doctoral Committee **Annija Sturmane**

ISBN 978-9934-18-620-2

Abstract

As the demand for higher bandwidth telecommunication systems grows, new technological approaches for information and communication systems are necessary. Great attention has been given to an all-optical telecommunication system due to the existing electro-optical system reaching its limits. For such a system to be implemented, one of the most essential aspects is nonlinear optical materials that can enable interaction between photons – mainly Kerr and Two-photon absorption (2PA) effects. At this moment material selection is the main bottleneck for all-optical telecommunication system implementation.

Material selection can be either carried out by experimental work or by quantum chemical calculations (QCC). But both of these approaches have the same underlying problem – the credibility of results. This gives rise to the problems studied in this work:

- How to correctly measure the Kerr and the 2PA effects of organic materials by separating them from other effects that induce similar responses to light in materials?
- How correct are QCC and how well they fit experimental measurements?

The first problem was studied by considering the Z-scan method for nonlinear optical properties characterization. For this chloroform and two organic compounds – DMABI and MeSBI dissolved in chloroform – were studied using a polarization-resolved Z-scan method with a picosecond laser, and nanosecond laser with variable pulse repetition rate. This allowed pinpointing a specific measurement methodology to determine the magnitude of Kerr effect electronic contributions of organic compound that is dissolved in a solvent using 30 ps laser.

To study QCC credibility Kerr and 2PA effects of 27 different organic compounds were measured and acquired results compared to QCC predictions by Gaussian 09. It was shown that linear polarizability values given by QCC can be used to predict experimental values of molecular reorientation contribution to the Kerr effect. Also, second-order hyperpolarizability values were calculated from Kerr coefficient values and compared to QCC results and two distinctive trends were observed. For molecules that did not possess any significant 2PA a linear relation between QCC results and experimental values for second-order hyperpolarizability was observed. On the other hand for materials that possessed experimentally observable 2PA effect the ratio of experimental value to calculation results was linearly dependent on two-photon absorption cross-section, indicating that the implemented calculation method is not sufficient enough in predicting two-photon contribution to Kerr response.

Contents

Introduction

Motivation

Through the years few numbers of experimental methods for third-order nonlinear optical characterization have established them self's as the base for material characterization. The main two methods have been the Degenerated four-wave mixing[1] and Z-scan[2]. Nowadays the Z-scan method is the most popular mainly due to the simple experimental setup and possibility to measure the Kerr and the Two-photon absorption effects simultaneously. Even though this method has been around since 1990 new publication regarding the Z-scan measurement methodology is being published in 2020 trying to establish a unified method for interpretation of the Z-scan measurements.[3] The main issue here is that the Kerr effect is measured through refractive index changes. At the same time, it is not the only effect that can induce refractive index changes of materials and the Kerr effect needs to be correctly separated from others, mainly from the thermo-optical contribution. The problem with the thermo-optical effect is that it can lead to refractive index changes through single laser pulse contribution or accumulative effects, even further complicating the separation. Also, the Kerr response can be separated into multiple contributions of which only electronic is of interest for high-bandwidth all-optical applications. All these aspects have different responses to laser pulse repetition rate, laser pulse width, and optical polarization of the light beam that is compiled in Table A. In literature nonlinear optical properties are measured using CW lasers as well as ns, ps, and fs lasers with pulse repetition rates from 1–40 000 Hz complicating correct comparison between materials studied by different scientific groups. Another approach to this problem could be finding some other experimental approach to Kerr effect measurements. One such alternative could be Mach-Zehnder interferometer that has been widely used for electro-optical effect measurements[4]. As there are only a few publications regarding the Mach-Zehnder interferometer for Kerr effect measurements, more research is necessary to conclude if this method could be an alternative.

Another essential problem for finding efficient nonlinear optical materials is finding a fast way for material screening for applicability. Although many papers regarding organic materials nonlinear optical properties have already been published, this is still a very active scientific field. But finding novel nonlinear optical organic materials by systematic experimental measurements is too time-consuming. To reduce the amount of experimental work for material selection, scientists have long worked to derive theoretical guidelines to structure-property relations of organic molecules. This includes generalized Miller's rule for extension of second-order susceptibility over spectral range[5],

Table A: *Thermo-optical and Kerr effect dependence on laser parameters. "Yes" means that effect is specific parameter dependent while "No" – effect is independent of specific parameter.*

Effect	Contributions	Pulse repetition rate	Pulse width	Lights polarization
Thermo-optical	Single-pulse	No	10^{-9} 10^{-8}	No
	Accumulative	Both are connected (40 kHz for 150 fs; 500 Hz for 15 ns)		No
Kerr	Electronic	No	10^{-15}	Yes
	Libration	No	10^{-13}	Yes
	Collision	No	10^{-13}	Yes
	Reorientation	No	10^{-12}–10^{-11}	Yes

further continuation, and experimental verification of this rule for third-order susceptibility[6–8], Ducuings observation of π-conjugated materials as promising for nonlinear optical applications[9–11] and others. While there are numerous papers regarding different structural-property relation studies[12–16], over-all knowledge is still insufficient for theoretical designing of nonlinear optical chromophores. Another solution could be Quantum Chemical calculations to predict hypothetical molecules nonlinear optical properties. This could allow shifting most of the material development from experimental to theoretical work by simpler structure screening. Although different Quantum Chemical calculations methods have already been employed for calculations of molecular linear optical as well as for nonlinear optical properties, there still isn't a widely accepted approach to calculations of the third-order nonlinear optical properties of organic materials.

Aim of the study

The main goal of this work is to establish a correct methodology for the third-order nonlinear optical effect studies using the Z-scan method and see how well values of refractive index changes acquired with Quantum Chemical

calculation corresponds to experimental values. This will be done by carrying out the following tasks:

- Study how the Z-scan measurements are influenced by laser pulse width, pulse repetition rate, and polarisation,
- Compare the Z-scan method to the Mach-Zehnder interferometer to establish in which situations each of the methods is more applicable,
- Carry out the Z-scan measurements for 27 organic compounds to study structure-property relation of these molecules,
- Compare acquired experimental results to the Quantum Chemical calculations results.

Author's contribution

The experimental setups presented in this work were mainly constructed by the author of this work, excluding custom-built electronic parts that were made by a colleague Janis Busenbergs. The author prepared all of the samples studied in this work and carried out optical absorption measurements for sample characterization. All of the nonlinear optical measurements with both the Mach-Zehnder interferometer and the Z-scan methods were done by the author. The Quantum Chemical calculations were carried out by colleague Igors Mihailovs.

All of the data processing, including writing MatLab or Python codes for data fitting, and result interpretation were done by the author.

Scientific novelty

This work presents an outline for a correct approach for correct interpretation of refractive index changes induced by optical irradiation. This includes separation of thermo-optical effects and Kerr effect separation and decomposition of the Kerr effect into electronic and molecular contributions when using the Z-scan method by employing polarization-resolved measurements.

A nonlinear optical property characterization of multiple novel organic materials is presented in this work that has not been previously studied, with some exhibiting large two-photon absorption values that could be used for optical limiting applications.

A correlation between the two-photon absorption effect in organic materials and how much the experimental values for the Kerr effect differs from the Quantum Chemical calculations carried out by Gaussian 09 has been presented. This correlation is shown to be independent of the organic material group.

1. Literature Background

1.1. Third-order susceptibility

Materials polarization can be written as polynomial dependence on the external electrical field:

$$P(t) = P_0 + \chi^{(1)} \cdot E(t) + \chi^{(2)} \cdot E^2(t) + \chi^{(3)} \cdot E^3(t) + \cdots \quad (1.1)$$

where the third-order term can be written as:

$$P^{(3)}(t) = \chi^{(3)} \cdot (E \cdot \cos(\omega \cdot t))^3 = \frac{\chi^{(3)} \cdot E^3 \cdot \cos(3\omega \cdot t)}{4} + \frac{3 \cdot \chi^{(3)} \cdot E^3 \cdot \cos(\omega \cdot t)}{4} \quad (1.2)$$

From this equation two different ways the material can interact with light can be derived: i) material response with the frequency of 3ω due to an electrical field with the frequency ω, ii) nonlinear response with the frequency ω of the incident electric field. Considering materials response with frequency ω, polarization can be expressed as:

$$P(t) = \chi^{(1)} \cdot E \cdot \cos(\omega \cdot t) + \frac{3}{4}\chi^{(3)} \cdot E^3 \cdot \cos(\omega \cdot t) = \chi_0 \cdot E \cdot \cos(\omega \cdot t), \ where \ \chi_0 = \chi^{(1)} + \frac{3}{4}\chi^{(3)} \cdot E^2 = \chi^{(1)} + \chi^{(3)}_{eff} \cdot I \quad (1.3)$$

where I is the optical intensity. In the general case the third-order susceptibility is written as forth-rank tensor:

$$\chi^{(3)}_{ijkl}(\omega_\sigma; \omega_1, \omega_2, \omega_3) \quad (1.4)$$

where i,j,k,l indicates the tensor element, ω_1, ω_2, and ω_3 are the incident photon frequencies and ω_σ characterizes the interaction between incident photons. Each of the possible three-photon interactions is defined by specific third-order susceptibility with some examples shown in Table 1.1.

Table 1.1: *Third-order susceptibility notation for different effects*

Effect	Third-order susceptibility notation
Three wave mixing	$\chi^{(3)}(\omega_1 + \omega_2 + \omega_3; \omega_1, \omega_2, \omega_3)$
Third-Harmonic generation	$\chi^{(3)}(3\omega; \omega, \omega, \omega)$
Optical Kerr effect	$\chi^{(3)}(\omega; \omega, \omega, -\omega)$
DC Kerr effect	$\chi^{(3)}(\omega; \omega, 0, 0)$

Third-order susceptibility characterizes materials macroscopic reaction to the electrical field and does not give us any information about this interaction on a molecular or atomic scale. For this, we introduce hyper-polarizability. For third-order interaction, we use the second-order hyper-polarizability. This parameter is then connected to third-order susceptibility through relation[17]:

$$\chi^{(3)}(\omega_\sigma; \omega_i, \omega_j, \omega_k) = \sum_p \sum_{i,j,k,\sigma} L^{(p)}_{i,j,k,\sigma}(\omega_\sigma; \omega_i, \omega_j, \omega_k) \cdot \langle \gamma^{(p)}_{i,j,k,\sigma} \rangle \quad (1.5)$$

where $\gamma_{i,j,k,\sigma}$ is the second-order hyper-polarizability and $L_{i,j,k,\sigma}$ is the local-field factor. The first sum in equation (1.5) is over all the microscopic elements of the system (atoms, molecules, molecular bonds, etc.). The second sum is over all frequencies present in the material.

To theoretically characterize NLO properties one of the most popular approaches is Sum over States (SOS) quantum theory. The description given further will be based on these works of literture[18,19]. In general, this theory uses the perturbation method to derive nonlinear susceptibility from the dipole operator matrix and the energy eigenvalues of the Hamiltonian. Most commonly two approaches are used for organic molecules characterization - two-level or three-level systems. A two-level system can be used to describe molecules with permanent dipole moment while a three-level system needs to be used for centrosymmetric molecules. In specific cases, the three-level system is extended to a five-level system differencing between singlet and triplet states for a specific excited level.

In reality, a combined system of both two-level and three-level systems are used to characterize materials. The most widely applied model in organic material studies is a simplified three-term equation[20]:

$$\gamma_{xxxx} \propto \frac{\mu_{ge}^2 \cdot \Delta\mu_{eg}^2}{E_{ge}^3} - \frac{\mu_{ge}^4}{E_{ge}^3} + \sum_{e'} \frac{\mu_{ge}^2 \cdot \mu_{ee'}^2}{E_{ge}^2 \cdot E_{ge'}}, \tag{1.6}$$

where the first term is called the D term (dipolar term, which is zero for centrosymmetric systems), the second is the N term (negative term due to sign) and the third – the T term (two-photon term) (see Figure 1.1).

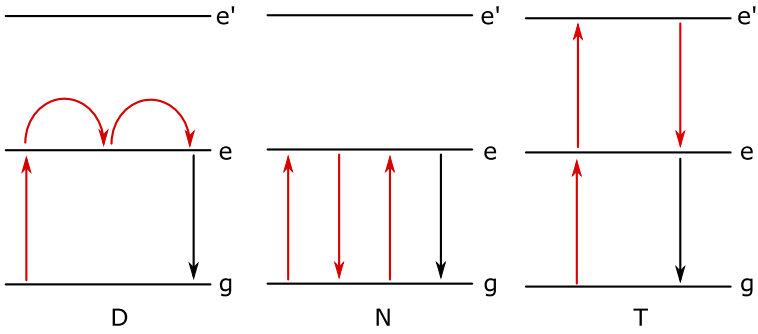

Figure 1.1: *Illustration of second-order hyperpolarizability terms – D (Dipolar term), N (Negative term) and T (Two-photon term). Red arrows indicate photons that influence material while the black lines indicates the observed photon and g is ground state while e and e' – excited states.*

1.2. Intensity effects

Now let's focus on how to connect third-order susceptibility with changes in materials optical properties. First, let's consider how the refractive index is related to the third-order susceptibility[21]:

$$\begin{cases} n_2 = n_{2;Re} + i \cdot \frac{\alpha_2 \cdot \lambda}{4\pi} \\ \chi^{(3)} = \chi^{(3)}_{Re} + i \cdot \chi^{(3)}_{Im} \\ n = n_0 + \frac{3}{4} \frac{\chi^{(3)} \cdot I}{{n_0}^2 \cdot \varepsilon_0 \cdot c} \end{cases} \rightarrow \begin{cases} \chi^{(3)}_{Re} = \frac{4 \cdot {n_0}^2 \cdot \varepsilon_0 \cdot c}{3} \cdot n_2 \\ \chi^{(3)}_{Im} = \frac{{n_0}^2 \cdot \varepsilon_0 \cdot c \cdot \lambda}{3 \cdot \lambda} \cdot \alpha_2 \end{cases} \tag{1.7}$$

where λ is the wavelength, c is the speed of light, ε_0 is the dielectric constant of vacuum, n_0 is the materials linear refractive index and n_2 is the nonlinear refractive index. To better compare the nonlinear refractive index properties on a molecular scale, the nonlinear refractive cross-section can be used, defined as[22]:

$$\delta_{\mathrm{NLR}} = \frac{\hbar \cdot \omega \cdot \mathrm{k} \cdot \mathrm{n}_2}{\mathrm{N}} \cdot 10^{58}, \tag{1.8}$$

Here the acquired value's unit of measure is the refractive Göppert-Mayer (RGM). In the case of the Kerr effect in isotropic media when all of the incident frequencies are equal media possesses only two independent tensor elements χ_{1122} and χ_{1221} and can be written as:

$$\chi^{(3)}_{ijkl} = \chi^{(3)}_{1122} \cdot \left(\delta_{ij} \cdot \delta_{kl} + \delta_{ik} \cdot \delta_{jl}\right) + \chi^{(3)}_{1221} \cdot \delta_{il} \cdot \delta_{jk} \tag{1.9}$$

Also, when considering a light beam of an arbitrary polarization, it can be shown that the NLO response will depend on amplitudes of circular-polarization components of this beam:

$$\begin{cases} \chi^{(3)}_{\pm} = A \cdot \left|E_{\pm}\right|^2 + (A + B) \cdot |E_{\mp}|^2 \\ n_{\pm} = n_0 + \frac{2\pi}{n_0} \cdot \left[A \cdot \left|E_{\pm}\right|^2 + (A + B) \cdot |E_{\mp}|^2\right] \end{cases} \tag{1.10}$$

where "+" denotes the right-handed rotation and "–" denotes the left-rotation. Induced refractive index changes will depend on how elliptic is the light's polarization with values between:

$$\begin{cases} n_{2;linear} = \frac{2\pi}{n_0} \cdot \left(A + \frac{B}{2}\right) \cdot |E|^2 \\ n_{2;circular} = \frac{2\pi}{n_0} \cdot A \cdot |E|^2 \end{cases} \tag{1.11}$$

By knowing refractive index changes in both of these cases, we can calculate coefficients A and B and know the values to third-order susceptibilities tensor elements. This is essential as the ratio of coefficients A and B can allow determining the mechanism involved in inducing refractive index changes (see Table 1.1)[23].

Table 1.1: *Parameters B/A ratios and corresponding mechanisms inducing refractive index changes*

Ratio B/A	Inducing effect	Response time, s
6	Molecular reorientation	10^{-12}
1	Non-resonant electronic response	10^{-15}
0	Electrostriction, thermo-optical	10^{-9}

1.3. Nonlinear refractive index

In general, all materials possess a nonlinear refractive index that varies from an order of 10^{-20} m^2/W for water till 10^{-4} m^2/W for complex organic thin films. For each material, these values can be separated into multiple contributions that represent different inducing mechanisms – electronic response, molecular reorientation, electrostrictive, thermal processes, and others. These effects can be experimentally separated by their response time.

Electronic contribution. This mechanism is based on a bound electron response on the applied optical field and is associated with the Kerr effect. Compared to other mechanisms electronic contribution is relatively small but it is present in all dielectric materials and has the fastest response time. It has been shown that π electron delocalization can greatly increase the magnitude of electronic contribution. Its contribution can also be enhanced by using the electrical field close to the materials resonance frequency, although this leads to an increase in absorption effects that in many cases can be unwanted.

Molecular effects. Depending on the literature source this contribution can be further separated into ether libration, collision, and reorientation processes)[24] (Reichert's approach) or vibration and reorientation[18] (Kuzyks' approach). First, let's consider Reichert's approach:

- *Libration* – This process is often described as molecule "rocking" in a potential well. The essential condition for this is that excitation pulse is shorter than molecules lifetime in this potential well (usually around 150 fs). Mainly asymmetrical molecules exhibit this effect.
- *Collision* – For both symmetrical and non-symmetrical molecules dipole induced dipole interaction influence neighboring molecules[24,25]. In solution, molecules are packed relatively close and dipole-dipole interaction occurs as an electronic overlap of neighboring molecules. This contribution is usually small (<10%) of overall NLO response and has a time constant of around 450 fs.
- *Diffusive reorientation* – This can be viewed as the next step of the libration process when a molecule is excited from one potential well to

another[26] and has a time constant around 1.5 ps. This response is exhibited only by anisotropic structures. A general equation for materials with different polarizabilities in each of directions has been presented by D. H. Close and his group in their 1966 paper[27]. This equation is of the form:

$$n_2 = \frac{\pi \cdot N}{45 \cdot n_0} \cdot \left(\frac{n_0^2+2}{3}\right)^4 \frac{((\alpha_2-\alpha_1)^2+(\alpha_3-\alpha_1)^2+(\alpha_3-\alpha_2)^2)}{k_B \cdot T} \qquad (1.12)$$

Another approach to separation of Molecular effects is simply into vibrational and reorientation effects. As reorientation has already been presented let's look at vibrational mechanisms:

- *Vibration* – Inner molecular vibrations associated with infra-red absorption. Vibrational effects have a time constant that corresponds to vibrational frequencies of molecules that are usually faster than reorientation[18]. In general, for third-order NLO effects, vibrational contributions are divided into four parts denoted as $[\mu^4]$, $[\alpha^2]$, $[\alpha\mu^2]$, and $[\mu\beta]$ where μ denotes dipole contribution, α denotes polarizabilities contribution, and β – first-order hyperpolarizabilities contribution[28]. Due to similar dependence on $[\alpha^2]$ as reorientation, they can be mixed together.

The difference in both approaches can be seen in Figure 1.2.

Electrostrictive contribution. This mechanism is based on molecular displacement due to inhomogeneous optical intensity in the material. If some intensity pattern with bright and dark fringes is formed in the media, a force will be applied on dipoles moving them into regions with higher optical intensity.

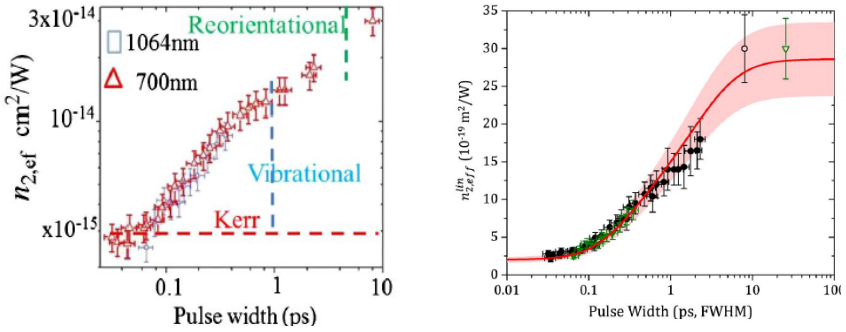

A **B**

Figure 1.2: *Different interpretations of same experimental results. A – M.G. Kuzyks approach in Ref [18]. B – M. Reichert approach in Ref [24]. Both graphs have been taken from the original papers. Approach A seperates results into thress different levels indicating atleast two step functions, while B use a single step function to approximate all data.*

Thermal effects. Another mechanism behind the nonlinear refractive index is through thermal effects. High-intensity optical irradiations can heat media leading to density changes thus inducing refractive index changes. Mainly three different types of thermal effects can be distinguished:

- *Single-pulse* – When optical light pulse length is longer than the time in which media can dissipate heat, a single laser pulse can induce thermos-optical effects. Depends on laser pulse width.
- *Accumulative* – If the time between two consecutive laser pulses is short enough, absorbed energy will accumulate and lead to thermal effects. Depends on pulse repetition rate with different critical repetition rates for specific pulse widths.
- *Thermal equilibrium* – Media has been heated to a state when absorbed and dissipated heat is in balance. At this point, it can be stated that the media "sees" laser pulse as continuous irradiation.

1.4. Two-photon absorption

In previous chapters, we concluded that as refractive index is a complex number with an imaginary part characterizing optical absorption. Similarly, as for the nonlinear refractive index, it can be shown that absorption also changes linearly from the optical intensity in case of third-order NLO effects:

$$\alpha = \alpha_0 + \alpha_2 \cdot I \tag{1.13}$$

where α_0 is the linear absorption and α_2 is the nonlinear absorption, also known as two-photon absorption (2PA) coefficient. A simple way to understand this process is to view it as the absorption of two photons at the same time. This leads to absorption changes proportional to the intensity at optical irradiation. While the 2PA coefficient characterizes media properties, often we need to describe a single molecule contribution to over-all absorption changes. In this 2PA cross-section is used, defined as:

$$\sigma_{2PA} = \frac{\hbar \cdot \omega}{N} \cdot \alpha_2 \tag{1.14}$$

where $\hbar \cdot \omega$ is the photon energy and N is the molecule concentration per cm^3. 2PA is not the only nonlinear absorption effect that can influence absorption and distinguish between different effects is essential. Saturable absorption (SA), reverse saturable absorption (RSA), and excited-state absorption (ESA) can also significantly influence absorption[29–33].

2. Experimental section

2.1. Z-scan setup

The Z-scan method was first proposed by Sheik-Bahae in 1990[2]. Experimental measurements are carried out by focusing a laser beam on to sample and moving it along the optical axis while measuring the transmitted light. By measuring transmitted light at far-field ($d>>z_R$) we will observe changes in beam parameters from sample position. In the case of the Kerr effect, a change in beam size will be induced that can be detected by a detector with a small aperture ($S_{aperture}<<S_{beam}$) before it is denoted as a "closed-aperture" detector. The 2PA effect will change samples absorption as a function from laser intensity. This will lead to power changes in transmitted light that can be measuring the overall power of the transmitted beam denoted as "open-aperture" measurement. In many cases, samples possess both effects – 2PA and Kerr effect. In general, it is assumed that open-aperture measurements will only detect absorption changes, while closed-aperture measurements are influenced by both effects. To separate the Kerr effect from the 2PA effect, closed-aperture data are divided by open-aperture data. Analytically Z-scan experiment can be described using the "thin-sample" model, where samples thickness is smaller or comparable to Rayleigh length[34]:

$$\begin{cases} Open-aperture \ \rightarrow \ T(z) = \sum_{k=0}^{\infty} \frac{\left(-\frac{q}{\left(1+\left(\frac{z}{z_R}\right)^2\right)}\right)^k}{(k+1)^{\frac{3}{2}}} \\ Closed-aperture \ \rightarrow T(z) = 1 - \frac{4\cdot\Delta\Phi\cdot\frac{z}{z_R}}{\left(\left(\frac{z}{z_R}\right)^2+9\right)\cdot\left(\left(\frac{z}{z_R}\right)^2+1\right)} \end{cases} \quad (2.1)$$

Parameter q and $\Delta\Phi$ are defined as:

$$\begin{cases} q = \alpha_2 \cdot L_{eff} \cdot I_0 \\ \Delta\Phi = n_2 \cdot k \cdot L_{eff} \cdot I_0 \end{cases} \quad (2.2)$$

where L_{eff} is the effective length and I_0 is the optical intensity at the focal point. These equations can be used when parameter $|q|<1$ and $|\Delta\Phi|<\pi$ (also known as weak nonlinear media condition).

The experimental setup used in this work is shown in Figure 2.1. Laser beam power was controlled using Fresnel Rhomb placed in a motorized rotation stage (SM 1) and Glan-Taylor prism. The e-ray of the prism was used in setup while the o-ray was directed towards a beam dump (BD). A small part of the laser beam was reflected with a beam splitter (BS) and measured using the reference detector (Ref). In this case, a glass substrate was used as a beam splitter. The laser beam was focused using a lens with an 11 cm focal length.

Transmitted light was measured using two detectors. Part of the transmitted beam was separated with a glass substrate (BS) and collected unto open-aperture detector (OA) using a lens with a 20 cm focal length to measure the power of the transmitted beam. The rest of the beam was transmitted through an aperture with a diameter of 1 mm and measured with a detector closed-aperture detector (CA). Aperture transmittance in this setup was estimated to be less than 1 % that fits very well for the "closed-aperture" measurement model. The sample was positioned on the motorized stage (SM 2) that moved parallel to the laser beam. Both motorized stages could be controlled using a computer. The experimental setup was built on a metal plate to move the setup between different laser sources. An option of placing a quarter-wavelength plate (QWP) was implemented into setup to carry out measurements with circularly polarised light.

To extend the Z-scan method for studying what Kerr contributions induce refractive index changes a $\lambda/4$ plate that changes beam polarization from linear to needs to be implemented[35,36]. In general case n_2 value as a function of the angle between the slow axis of $\lambda/4$ plate and linear polarization direction can be written as allowing to determine tensor coefficients A and B:

$$n_2 = \pi \cdot (2 \cdot A + B \cdot (\cos 2\theta)^2) \cdot \frac{|E|^2}{n_0} \qquad (2.3)$$

The following Z-scan measurements were carried out in this work:

1. Measurements with ns laser at different pulse repetition rates to study the influence of the thermo-optical effects,
2. Circular and linear polarisation measurements with ns laser to separate the thermo-optical and the Kerr contribution to refractive index changes,
3. Measurements with ps laser to study the Kerr and 2PA effects of different materials,

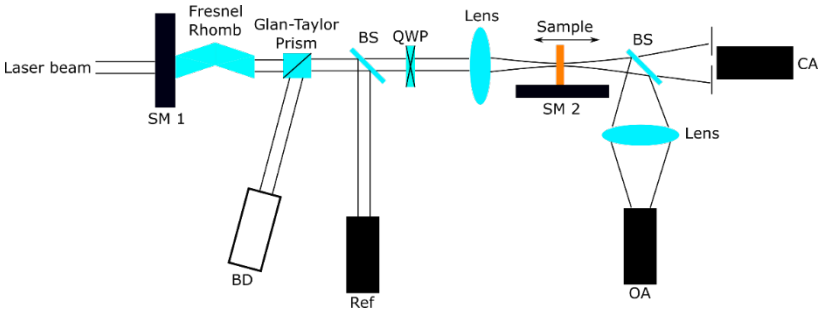

Figure 2.1: *Z-scan experimental setup. BD – Beam Dump; BS - Beam Splitter; QWP – Quarter-wavelength plate; SM – Step motor; Ref – Reference detector; CA – Closed-aperture detector; OA – Open-aperture detector.*

4. Ps measurements at different polarizations to study the origins of the Kerr effect and calculate values of different third-order susceptibility tensor elements.

Measurements were carried out with ns laser (Nd:YAG laser with 8 ns pulse duration and variable pulse repetition rate from 200-40 000 Hz was used (EKSPLA NL 640)) 30 ps laser (1064 nm an Nd:YAG laser with 30 ps pulse duration and 10 Hz repetition rate was used (EKSPLA PL 2143A)) and 15 ps tuneable laser (variable pulse repetition rate from 10 to 1000 Hz (EKSPLA PL2210 Picosecond laser/PG400 Optical Parametric Generator))

2.2. Mach-Zehnder interferometer setup

Mach-Zehnder interferometer (MZI) experimental setup consists of two mirrors and two beam splitters that separate incoming beam into two and then combine them again (see Figure 2.2) resulting in an interference pattern dependent on the phase difference between both beams:

$$I_{out} = \frac{I_1+I_2+2\cdot\sqrt{I_1\cdot I_2}\cdot\cos(\Delta\Phi)}{2} \tag{2.4}$$

where I_1 and I_2 are the optical intensity of the first and the second beam and $\Delta\Phi$ is the phase difference between both beams. No phase difference ($\Delta\Phi$=0) between both beams lead to constructive interference while the phase difference of $\Delta\Phi$=π/2 results in destructive interference.

In the case of a pulsed laser source path difference between both arms needs to be shorter than the coherence length of the laser to acquire a stable interference pattern. Coherence length can be calculated as:

$$L_C = \frac{\lambda^2}{n\cdot\Delta\lambda} \tag{2.5}$$

MZI measurements were carried out in two forms – a single beam setup and a two beam setup (see Figure 2.2). For both cases, the incoming beam was split into two beams using a beam splitter (BS) – sample and reference beams. The sample beam was guided through a lens that focused the beam onto the sample and through another lens that collimated the beam – both with a focal length of 8 cm. A motorized sample holder was placed in the focus of both lenses. To find the focal point Z-scan type measurement could be carried out using a reference detector (Ref 2) as a closed-aperture measurement. This insured that no beam size variation due to the Kerr effect should be present. A small part of the beam in the sample arm was separated using a glass slide and measured with a closed-aperture detector for two purposes: i) to measure any power changes that could be induced due to the 2PA effect; ii) detect beam size variation due to Kerr effect. An optical wedge was placed in reference beams way to adjust the optical path distance between both beams to be smaller than the coherence length

(very essential for ps laser measurements). To monitor the laser power part of the reference beam was separated using a glass slide and measured using a reference detector (Ref 1). Both beams were guided towards the second BS where they interfered. The output signal was measured using another detector (Int). In the case of the two beam measurements, optical filters that separated probing and inducing beams were placed in front of detectors. In this case, no special setup was used to control the power of the laser source as various different lasers were used and for each of them a different way to control laser power was used – some had an inbuilt power controller while for other optical filters were used.

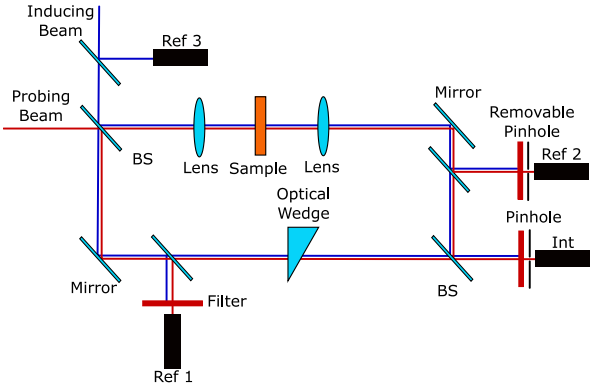

Figure 2.2: *MZI experimental setups. For single beam setup only probing beam was used. In two beam case both inducing and probing beams were used. BS – beam splitter. Ref and Int corresponds to different detectors.*

2.3. Quantum Chemical calculation parameters

The first step for the Quantum Chemical calculation (QCC) was calculating molecular structures. Spatial molecular structures were calculated in vacuum using all the ωB97X-D density functional with empirical atomistic dispersion correction and 6-311G(d,p) Pople-style basis set. Next, the first-order hyperpolarizability is calculated analytically using the Gaussian 09 coupled perturbed Kohn-Sham approach and then differentiated numerically using default settings to acquire values of second-order hyperpolarizability. CAM-B3LYP density functional was used with a 6-311G(d,p) base set. This base set means that internal electron orbital wavefunctions are expressed as six Gaussian functions with fixed parameters while valence orbital wavefunctions are expressed as three Gaussian functions with variable parameters. To calculate the solvent impact on the second-order hyperpolarizability CPCM continuum solvation model in the default nonequilibrium mode was used.

3. Results and Discussion

3.1. Evaluation of NLO measurement methods

3.1.1. Z-scan

Calibration. To calibrate the Z-scan setup, experimental measurements of chloroform and CS_2 solutions were carried out with 30 ps laser. For chloroform acquired value was $n_2 = (2.01 \pm 0.14) \cdot 10^{-15}$ cm^2/W and for CS_2 – $n_2 = (3.10 \pm 0.25) \cdot 10^{-14}$ cm^2/W. Both values fit well with literature[37] proving that a specific setup can be used to measure the Kerr effect.

Pulse width influence. A comparison of measurements implementing either of lasers was carried out using chloroform. Firstly, the sample was measured using 8 ns laser at 4 kHz repetition rate and compared to 30 ps measurement. Both experimental curves had inverse shapes. By calculating values of n_2 for both cases, it was observed, that ps measurements gave $n_2 = (2.01 \pm 0.14) \cdot 10^{-15}$ cm^2/W, while ns measurements gave $n_2 = (-4.47 \pm 0.23) \cdot 10^{-13}$ cm^2/W which has an opposite sign and much larger value than the Kerr coefficient for chloroform. This inconsistency can be explained by thermal effects. For chloroform heat dissipation time is $\tau_S = 15$ ns and the frequency at which accumulative thermal effects become significant is 500 Hz indicating that both effects are present.

Pulse repetition rate influence. To investigate this further, experiment implementing ns laser with different pulse repetition rates were carried out. Acquired n_2 values are shown in Figure 3.1. While experimental data approaches constant value at small laser pulse repetition rates, as expected, this value still has a negative sign that does not fit values presented in the literature indicating single-pulse contribution. The frequency dependence indicates that in these measurements thermal equilibrium was not reached.

Polarisation measurements. To the study origins of nonlinear refractive index changes in chloroform, measurements at different polarisations – varying from

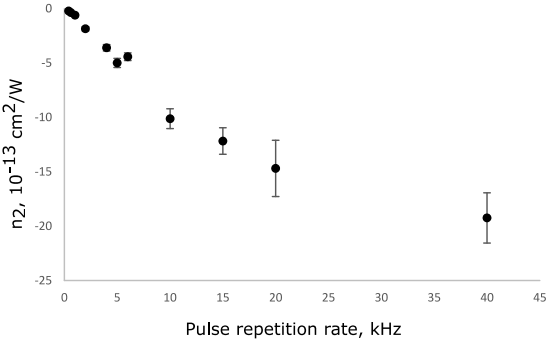

Figure 3.1: *Nonlinear refractive index of chloroform at different pulse repetition rates.*

circular to linear – was carried out using the 30 ps laser (see Figure 3.2). From acquired results, the *B/A* ratio was calculated giving a value of 6.09. This indicates that for pure chloroform this effect is solely due to molecular reorientation.

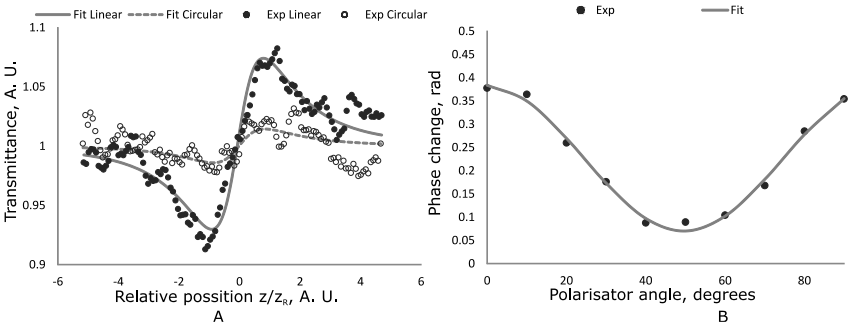

Figure 3.2: *Experimental measurements at different polarisations. A – The transmittance curve drastically changes when comparing linear and circular polarisation measurements. B – To determine B/A ratio, phase changes were plotted as a function of Polarizers angle and fitted with equation (2.3).*

Similar measurements were also carried out using ns laser at different repetition rates to distinguish between the Kerr and thermo-optical contributions to refractive index changes as both of these effects have different dependencies on polarisation. Experimental measurements were carried out with ns laser at a 200 Hz pulse repetition rate. To separate the thermo-optical and Kerr contributions, it was assumed that for the thermo-optical effect $B/A = 0$ and for the Kerr effect $B/A = 6$. This means that any difference in refractive index changes between values at linear and circular polarizations is only due to the Kerr effect. Using this assumption thermo-optical effect contribution was calculated to be $n_{2;TO} = (-7.56 \pm 0.65) \cdot 10^{-15}$ cm^2/W and Kerr contribution to be $n_{2;Kerr} = (1.84 \pm 0.31) \cdot 10^{-15}$ cm^2/W. The acquired Kerr value is close to the ps measurement value, validating that polarization-dependent measurements can be used to separate both contributions. But this method is limited by the laser repetition rate. When increasing the laser pulse repetition rate up to 1000 Hz any distinguishable dependence on polarization disappeared, due to a strong thermo-optical effect.

Study of organic dyes. In this section guidelines of result analysis for samples consisting of organic chromophore dissolved in a solvent will be given. Two organic compounds were chosen – DMABI and MeSBI (Structural formulas will be shown later in Fig. 3.7). These molecules were chosen as they possess

insignificant absorption at 532 nm and the 2PA effect should not influence experimental measurements (absorption properties of these compounds will be presented in section NLO properties of organic molecules).

Firstly Z-scan measurements for these compounds were carried out using 30 ps laser to determine the Kerr coefficient for these molecules. The acquired values were $n_2 = (2.49 \pm 0.22) \cdot 10^{-13}$ cm^2/W for DMABI and $n_2 = (2.52 \pm 0.62) \cdot 10^{-13}$ cm^2/W for MeSBI. For DMABI polarization-resolved Z-scan measurements with 30 ps were also carried out. In this case, B to A ration was calculated to be $B/A = 4.39$. By assuming that for pure chloroform $B/A = 6.09$, the ratio value for the DMABI molecule was calculated to be $B/A = 2.85$. This was acquired by solving the following equation:

$$\frac{1}{2} \cdot \left(\frac{B}{A}\right)_{(Exp)} + 1 = \frac{n_{2;(C)} + n_{2;(Organic\ Dye)}}{\frac{1}{\frac{1}{2}\left(\frac{B}{A}\right)_{(C)}+1} \cdot n_{2;(C)} + \frac{1}{\frac{1}{2}\frac{B}{A}+1} \cdot n_{2;lin(Organic\ Dye)}} \rightarrow$$

$$\begin{bmatrix} \left(\frac{B}{A}\right)_{(Exp)} = 4.39 \\ \left(\frac{B}{A}\right)_{(C)} = 6.09 \end{bmatrix} \rightarrow 3.95 = \frac{n_{2;(C)} + n_{2;(Organic\ Dye)}}{\frac{1}{4.045} \cdot n_{2;(C)} + \frac{1}{\frac{1}{2}\frac{B}{A}+1} \cdot n_{2;lin(Organic\ Dye)}} \quad (3.1)$$

For further result analysis assumption is made that only molecular reorientation and electronic components influence refractive index changes induced by DMABI, with molecular reorientation having ration $B/A = 6$ and electronic response $B/A = 1$. Using this assumption, the measured n_2 value was separated into both components and refractive index values were calculated to be $n_{2;MR} = 1.52 \cdot 10^{-13}$ cm^2/W and $n_{2;E} = (9.71 \pm 0.22) \cdot 10^{-14}$ cm^2/W. These values will be further used in comparison with QQC results to estimate how precise calculations can predict experimental results.

Errors of organic chromophore measurements with ns laser. The main issue with NLO measurements implementing ns laser is the thermo-optical effect due to either one- or two- photon absorption. This would mean that for materials that possess insignificant absorption at irradiation wavelength λ and $\lambda/2$, correct measurements of the Kerr effect should be possible with ns laser. To check this DMABI and MeSBI solutions were measured with ns laser. Firstly MeSBI was measured with ns laser at a 40 kHz repetition rate. For MeSBI calculated refractive index changes were $n_2 = (-2.8 \pm 0.3) \cdot 10^{-10}$ cm^2/W that is few orders higher than the value measured with ps laser. By measuring n_2 dependence on polarisation, no variation in nonlinear refractive index value was observed. Also, experiments at different pulse repetition rates were carried out and observed that the magnitude of the nonlinear refractive index decreased with the repetition rate. This indicates that these changes are only due to thermal effects, even though MeSBI has no significant absorption at 1064 nm or 532 nm. This shows an important aspect of NLO measurements – even for materials with insignificant absorption at irradiance wavelength and at half of it, NLO properties can still be

dominated by thermo-optical effects. DMABI ns measurements gave a positive value of $n_2 = (1.3 \pm 0.2) \cdot 10^{-10}$ cm^2/W, which is around three orders larger than the value acquired with 30 ps laser. Polarisation-resolved measurements gave a *B/A* ratio of 1.18 for DMABI, indicating that mostly electronic contribution dominates refractive index changes. This will be analyzed in further sections at this moment remaining as an open problem – why does Kerr effect electronic contribution for DMABI increase with pulse duration?

Summary. In conclusion, a wide spectrum of different measurements was carried out to test the limits of the Z-scan method for measuring the Kerr effect of liquids. The main conclusions from these sections are:

1. While ns laser pulse width should not be long enough to induce a thermal response from liquids, at a higher repetition rate this happens due to the accumulative thermo-optical effect and overwhelms the Kerr effect. This can lead to overestimation of the Kerr effect if not investigated properly,
2. While in some cases Kerr effect contribution can be separated from the thermo-optical one using polarization-resolved Z-scan measurements, it is still a very limited method. For 8 ns pulse width laser, it was possible to separate both contributions up to 1 kHz repetition rate,
3. Polarisation-resolved Z-scan measurements can be used to determine the ratio of molecular and electronic contributions to the Kerr effect to some extent. Theory suggests that collision and electronic effects will have a *B/A* ratio of 1 while libration and diffusive reorientation *B/A* ratio will be 6. While collision effects are very profound when studying solvents, time-resolved measurements of specific organic compounds dissolved in solvent have shown that no collision effects are present due to organic compound[38]. This can be assumed only for low concentration solutions when the organic dye has a much larger Kerr effect than the solvent. A more complicated aspect is the separation of libration and diffusive reorientation and would demand pulse width dependent measurements.
4. When measuring solutions of organic compounds dissolved in chloroform with ns laser, it is not straight forward answer whether the response is due to thermo-optical effects or the Kerr effect. Measurements showed that it also does not correlate with linear absorption at irradiance wavelength or the 2PA effect.

3.1.2. Mach-Zehnder interferometer

For single beam MZI measurements of chloroform were carried out using three different lasers – 30 ps laser, ns laser, and 473 nm CW laser.

Ps measurements. Measurements with ps laser were carried out to confirm that this setup can be used to study the Kerr effect. During experimental testing, there were difficulties to acquire a stable interference pattern due to short coherence length (I = 1.47 mm). To overcome this, the experimental setup was constructed so that both arm lengths were equal and an optical wedge was used to compensate path difference introduced by the quartz cell. An example of experimental data can be seen in Figure 3.3. Kerr coefficient was measured to be $n_2 = (2.09 \pm 0.18) \cdot 10^{-15}$ cm^2/W which is similar to values presented in the literature.

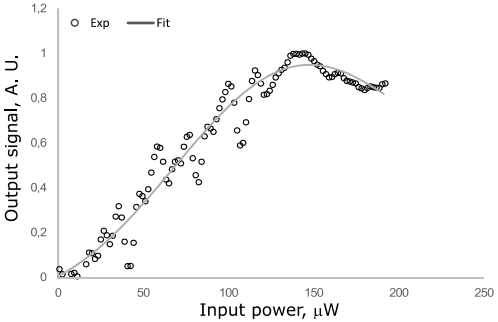

Figure 3.3: *MZI experimental data using 30 ps laser.*

Ns measurements. An example of experimental measurement can be seen in Figure 3.4 A. Here a phase change larger than 4π was measured. Measurements were carried out at different laser repetition rates. Acquired results were compared with Z-scan results to verify their credibility. From Figure 3.4 B it is evident that results from both methods fit very well.

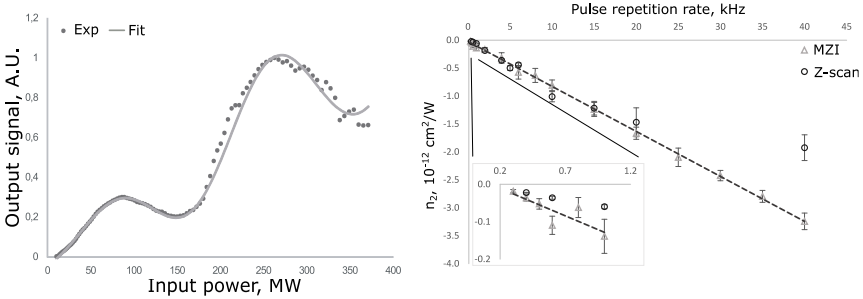

A **B**

Figure 3.4: *A – Experimental measurement of chloroform using single beam MZI. Dots represent experimental measurements and line represents an analytical fit. B – Pulse repetition rate measurements for both MZI and Z-scan method compared. Measured refractive index changes are similar with both methods.*

CW measurements. For further studies of equilibrium thermo-optical effect, measurements using 437 nm CW laser were carried out. An example of experimental measurements can be seen in Figure 3.5. For the CW case, we can assume that the sample has reached thermal equilibrium and we can calculate the nonlinear refractive index using values of chloroforms thermo-optical coefficient and linear absorption presented in literature[39,40]. This gave refractive index changes of $n_2 = -1.27 \cdot 10^{-8}$ cm^2/W. Experimental measurements gave value $n_2 = (-5.06 \pm 0.32) \cdot 10^{-8}$ cm^2/W that is of the same order as the theoretical value.

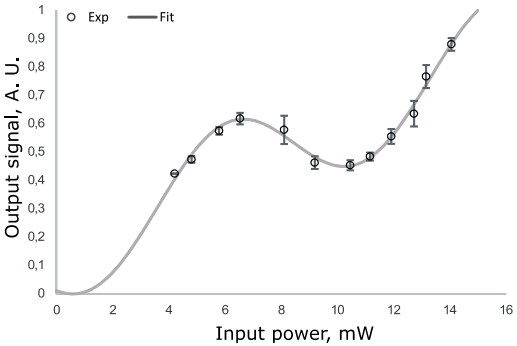

Figure 3.5: *MZI measurement using a 437 nm CW laser.*

The second part of MZI experiments used two laser beams for demonstration of all-optical switching using two beams – inducing and probing. Ns laser was used as an inducing beam while different CW lasers with wavelengths of 437, 632.8, or 780 nm were used as probing beams. Example of experimental data for 780 nm probing laser and ns laser at 30 kHz pulse repetition rate are shown in Figure 3.6. A. Experimental measurements were carried out at different repetition rates for all lasers and results can be seen in Figure 3.6. B.

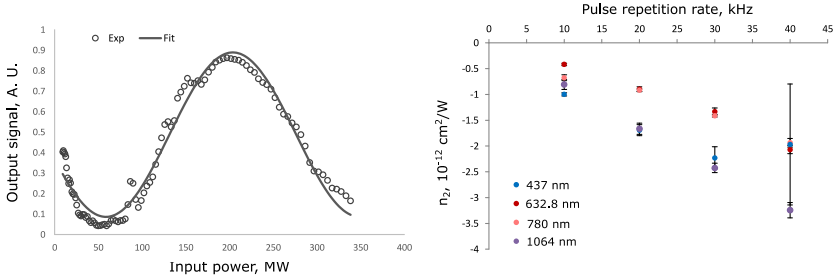

A **B**

Figure 3.6: *A – Experimental data of two-beam MZI measurement using 780 nm laser as probing and ns laser with pulse repetition rate at 30 kHz as inducing beam. B – Comparison of refractive index changes with different probing lasers.*

From experimental results it is evident that data with 437 nm probing laser are similar to single laser (ns laser) results, while 632.8 and 780 nm laser gave smaller n_2 values. This can be due to multiple factors: i) statistical error during approximation, ii) all lasers had different spot sizes in the focal point, iii) how precisely both beams were positioned respectively to each other and how well they overlapped. In Figure 3.6. B only the statistical error part is represented. Regarding the second aspect, all of the probing beams had smaller beam sizes in the focal point compared to the inducing beam.

A summary of measured nonlinear refractive index values at different pulse widths are shown in Table 3.1. In principle, this setup could be used to probe Kerr effect induced all-optical switching between two different laser beams and to determine $\chi(\omega_1;\omega_1,\omega_2,-\omega_2)$, although ps laser with few Hz repetition rate and fast detectors synchronized with the laser would be necessary.

Table 3.1: *Nonlinear refractive index values*

Laser	Dominant Effect	Value
CW laser	The equilibrium state of the thermo-optical effect	$-5.06\pm0.32\cdot10^{-8}$ cm^2/W
ns laser	Accumulative thermo-optical effect	Depends on laser repetition rate ($-0.0185\ldots-3.24\times10^{-12}$ cm^2/W)
ps laser	Kerr effect	$2.09\pm0.18\cdot10^{-15}$ cm^2/W

Summary. In conclusion, the MZI method was tested as an alternative to the Z-scan method for NLO measurements. The following conclusions were made:

1. During MZI measurements, induced phase change excided 4π. Compared to Z-scan that more complicated analytical models to processes measurements with large phase change ($>\pi/2$), MZI can use the same analytical model for wide range phase change values and are only limited by the change of location of sample position relative to the focal point at which no beam size variations are induced. This is a clear advantage over the Z-scan method.
2. By using short pulse lasers (ps range), coherence length becomes a limiting aspect for MZI measurements. While for 30 ps laser we were able to adjust the optical length of both MZI arms with an optical wedge, this could become more complicated if measurements are carried out with femtosecond laser. On the other hand, Z-scan has no such limitations.

3.2. NLO properties of organic materials

Z-scan measurements were carried out for three material groups: i) Aminobenziliden-1,3-indandione (ABI) derivatives (13 compounds). Due to a wide range of different derivatives, this material group could give some insight into specific structure-property relations of the Kerr and 2PA effects with main focus on different donor and acceptor groups; ii) Triphenylamine (TPA) derivatives (8 compounds). This group includes materials with small structural alterations to study how angular positions of different molecular groups influence NLO properties; iii) 2,6-bis(4-aminobenzylidene)-s-indacene-1,3,5,7-tetraones (BIT) derivatives (6 compounds). These materials exhibit a strong 2PA effect and could be applicable for optical limiting applications.

3.2.1. ABI derivatives

Compounds: Molecular structures, abbreviations, and absorption spectra for studied ABI derivatives are shown in Figure 3.7. The main structural variations between selected compounds can be summarized as follows: i) Molecules with the same indandione acceptor group but with different donor groups (DMABI-Ju, DAMBI-dph, DMABI, MeOBI, MeSBI, DMABI-OH, DMABI-Ph6); ii) Molecules with different amount of indandione acceptor groups attached to triphenylamino donor group (TPA – 0, DMABI-dph – 1; DiDMABI – 2; TriDMABI – 3). As TPA did not exhibit any significant absorption at the visible spectrum, absorption data for this compound is not presented. While none of the compounds possess significant absorption at 1064 nm, some of the molecules absorb 532 nm that could influence 2PA properties. As in this case, only molecules that do not possess any significant absorption at 532 nm are DMABI, DMABI-OH, MeOBI, and MeSBI it is expected that these molecules will have no 2PA effect.

NLO results: NLO properties for these compounds were measured using the 30 ps laser. Also to study pulse width influence on 2PA, some of the compounds with the most profound 2PA properties were also measured with ns laser. In this case, only open aperture data were studied as closed-aperture data was strongly influenced by thermo-optical effects due to absorption. Linear optical properties at 532 nm and acquired NLO values with ps and ns lasers are presented in Table 3.2.

Observation 1: The first main conclusion from these results is regarding the 2PA effect correlation with the linear absorption at 532 nm. A somewhat linear trend between both parameters can be seen (see Figure 3.8).

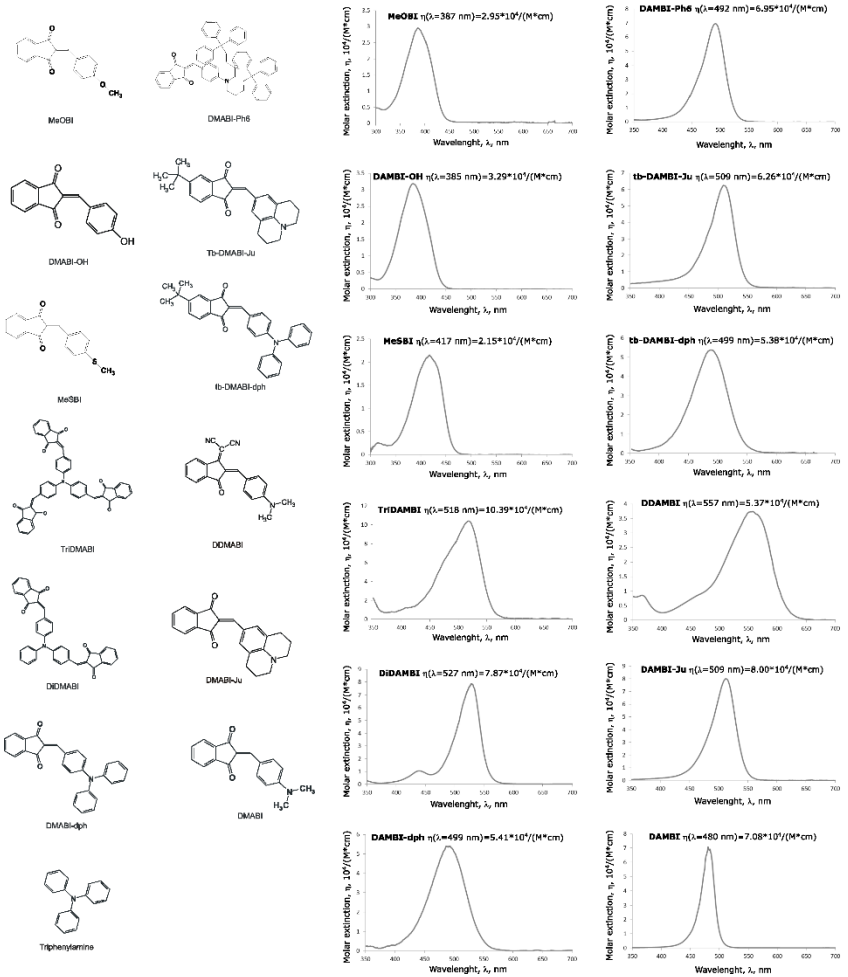

Figure 3.7: *Molecular structures,* abbreviation*s and absorption spectrums of ABI derivatives.*

Observation 2: Next we will look at material group TPA, DMABI-dph, DiDMABI, and TriDMABI. Both 2PA and nonlinear-refractive cross-section is plotted as a function from the ABI group number in Figure 3.9. This figure shows that 2PA cross-section increases linearly with the number of ABI groups while nonlinear refractive cross-section increase quadratically. This nonlinear

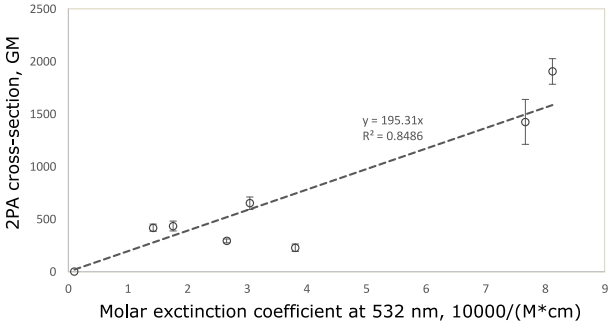

Figure 3.8: *Two-photon absorption cross-section at 1064 nm as a function from the molar extinction coefficient at 532*

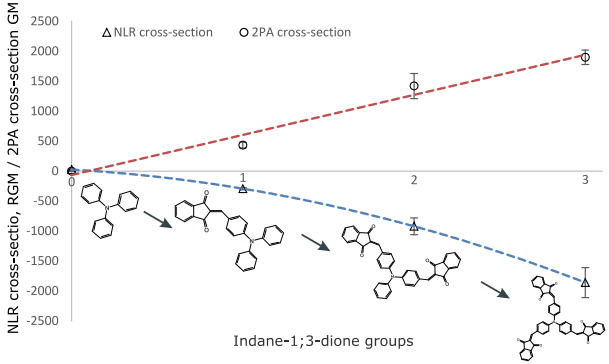

Figure 3.9: *Nonlinear refractive (NLR) cross-section and 2PA cross-section as functions of ABI groups.*

contribution could be through both the number of ABI groups increasing Dipolar contribution and 2PA increasing corresponding two-photon term of Kerr effect.

Observation 3: Lastly, when comparing ns and ps results for 2PA, it is evident that ns values are much larger (see Table 3.2). When looking at the difference between both values, it is around 10^3 that is close to the difference in laser pulse widths. This indicates that 2PA scales with pulse width. During Z-scan calibration, it was observed that the Kerr value for DMABI increases when comparing ns and ps measurements. As both 2PA values of various organic compounds and the Kerr effect of DMABI increased proportionally to pulse width (three orders of magnitude), this could indicate the two-photon term of Kerr effect value increase for DMABI. This is also supported by polarisation measurements indicating that mainly electronic contribution is present during ns measurements compared to ps measurements. This was further studied by spectral measurements of 2PA and Kerr effect for DMABI.

3.2.2. Spectral measurements

To better understand pulse duration influence on the Kerr effect and how feasible it is that for DMABI 2PA contribution to the Kerr effect is the reason

for the increase of Kerr effect with pulse duration additional experiment spectral measurements for DMABI were carried out study the Kerr and 2PA effect spectral dispersion. This was done using a 15 ps tuneable laser. Values of 2PA cross-section and nonlinear refraction cross-section are shown in Figure 3.10 for DAMBI. It can be seen that the Kerr effect changes its sign when approaching spectral diapasons where the 2PA effect can be observed – as observed for most ABI derivatives. Also, the tail of 2PA gives a positive contribution to the Kerr effect at larger wavelengths, explaining the increase of the Kerr effect with pulse length.

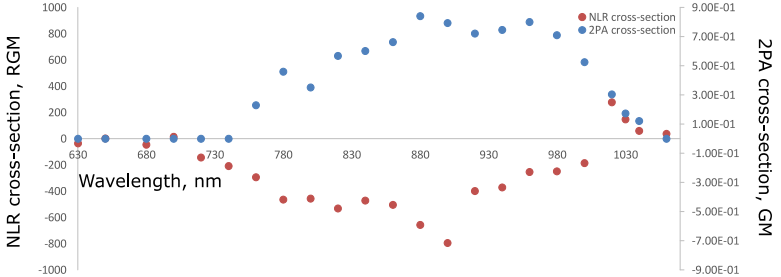

Figure 3.10: *Spectral dispersion of DMABI nonlinear refractive and two-photon absorption cross-sections spectral dispersions.*

3.2.3. TPA derivatives

Compounds: The next material group studied in this work was different TPA derivatives. This included materials with smaller or larger molecular groups attached to the TPA group. Structural forms as well as abbreviations for studied

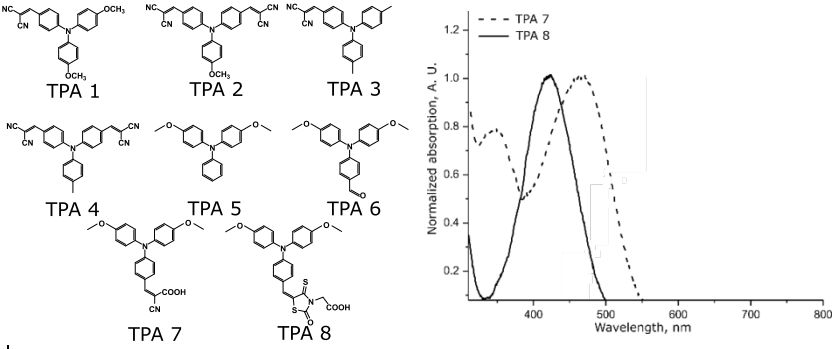

Figure 3.11: *Structural formulas and abbreviations of the TPA derivatives as well as absorption spectrums for TPA 7 and TPA 8.*

materials are shown in Figure 3.11. Only two of these compounds possessed any significant absorption at the visible range – TPA 7 and TPA 8 with a maximum for TPA 7 – 24000 1/(M·cm) at 424 nm; TPA 8 – 18000 1/(M·cm) at 466 nm. Also, only TPA 7 had significant absorption at 532 nm.

NLO results: Measured NLO values with 30 ps laser for all compounds are shown in Table 3.2. Only TPA 7 possessed any significant 2PA effect with a magnitude of $\alpha_2 = (7.10 \pm 0.86) \cdot 10^{-8}$ cm/W corresponding to $\sigma_{2PA} = 592 \pm 72$ GM.

Observation 1: To study these results in more detail QCC results of spatial structures of molecules were compared. The essential difference was in the angle between either methyl (TPA 3) or methoxy (TPA 1) groups to the central NC_3 group. TPA 1 had an angle of 68^0, while TPA 3 had 63^0. This could indicate that this angle is the main reason behind differences in the Kerr effect, as it influences the electron flow between molecular groups. On the other hand QCC results for TPA 2 and TPA 4 (followed the rule that molecule with a stronger donor group had a larger Kerr effect value), the molecular structure showed that none of the phenyl rings were close to being in-plane with the central group. This indicates that angles between molecular groups influence group conjugation and how much the strength of separate molecule groups influence overall molecular properties.

3.2.4. BIT derivatives

Compounds: The last molecule group studied in this work was 2,6-bis(4-aminobenzylidene)-s-indacene-1,3,5,7-tetraones (BIT) derivatives. First reports of NLO properties of such materials can be traced back to R. D. Breuker group[41] that presented novel material for NLO applications with high 2PA for optical limiting. In this work, specific derivatives of this base compound were studied that possessed stronger acceptor groups (dicyanomethylene), as well as 3-oxo-3-(2,2,2-triphenylalkoxy)propyl groups that allow forming higher-concentration homogeneous guest-host thin films to find more efficient materials for optical limiting applications. These molecules have a centrosymmetric structure of form D-A-D. Structures of studied compounds, abbreviations, and spectra can be seen in Figure 3.12. BIT 0 represents the original compound studied by R. D. Breuker group. NLO results are compiled in Table 3.2.

Observation 1: When looking at the acquired values, the molecules can be separated into two groups – negative Kerr effect (BIT 0, BIT 1, BIT 3, and BIT 5) and positive Kerr effect (BIT 2 and BIT 4). From a structural point of view, the main difference between these molecules is in the central acceptor group. While all molecules are centrosymmetric, molecules with negative Kerr effect

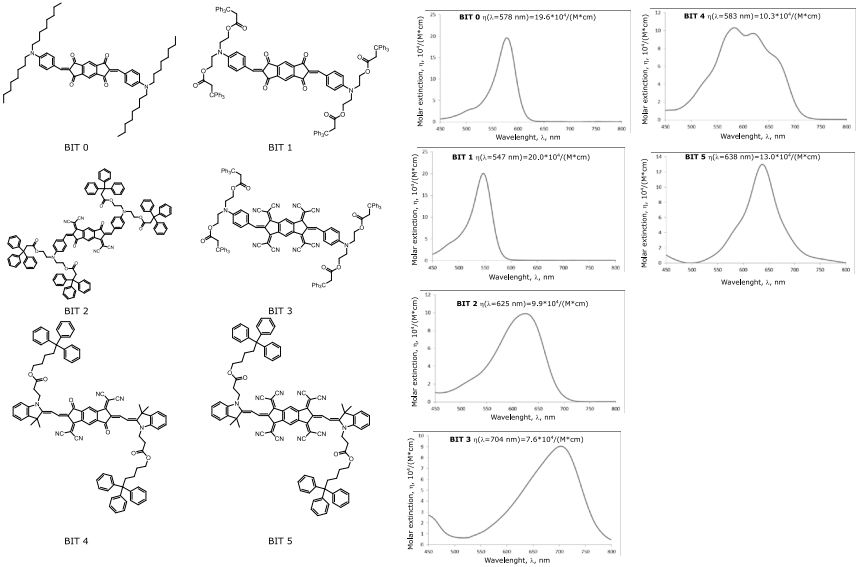

Figure 3.12: *Structures, abbreviations and absorption spectrum of studied BIT derivatives.*

have a central acceptor group with mirror symmetry while positive molecules lack this symmetry. This could be an indication that third-order NLO properties for these molecules are not only influenced by dipolar properties of the whole molecule, but also by dipolar and quadrupole properties of separate groups – in this case, the central acceptor group. There are two main ways to approach these results based on the three-level model:

1. State that the sign indicates on which side of two-photon resonance the measurements were done. This would mean that for BIT 0, BIT 1, BIT 3 and BIT 5 2PA resonance is at a longer wavelength, while for BIT 2 and BIT 4 has a shorter wavelength. This conclusion can be made if we assume that one-photon contribution is negligible.
2. On the other hand, we the sign of the Kerr effect for centrosymmetric molecule indicates which contribution – one- or two- photon – is dominant for the Kerr effect.

In reality, both of these statements are true and additional information regarding the spectral dispersion of 2PA is necessary for further analysis.

Table 3.2: *NLO coefficients of studied molecules.*

Solute	$\beta_{2;ps}$, cm/W · 10^{-7}	$\sigma_{2PA;ps}$, GM	$\beta_{2;ns}$, cm/W · 10^{-4}	$\sigma_{2PA;ns}$, GM·10^{6}
Chloroform	–	–	–	–
DMABI	–	–	–	–
Triphenylamine	–	–	–	–
DMABI-dph	0.519±0.056	434±47	–	–
DiDMABI	1.23±0.18	1420±210	1.044±0.090	3.23±0.28
TriDMABI	1.281±0.081	1900±120	1.74±0.16	5.41±0.51
tb-DMABI-dph	0.438±0.059	417±59	–	–
DMABI-Ju	0.332±0.054	228±37	–	–
tb-DMABI-Ju	0.365±0.024	293±19	0.480±0.029	1.491±0.090
DMABIOH	–	–	–	–
DDMABI	0.962±0.089	652±60	–	–
DMABI-Ph6	–	–	–	–
MeSBI	–	–	–	–
MeOBI	–	–	–	–
TPA 1	–	–	–	–
TPA 2	–	–	–	–
TPA 3	–	–	–	–
TPA 4	–	–	–	–
TPA 5	–	–	–	–
TPA 6	–	–	–	–
TPA 7	0.710±0.086	592±72	–	–
TPA 8	–	–	–	–
BIT 0	3.66±0.95	6629±1721	–	–
BIT 1	1.07±0.14	3846±523	–	–
BIT 2	2.99±0.31	11378±1182	–	–
BIT 3	1.09±0.17	4330±678	–	–
BIT 4	2.53±0.24	7320±700	–	–
BIT 5	1.09±0.10	3372±314	–	–

n_2, $cm^2/W \cdot 10^{-13}$	δ_{NLR}, RGM	γ_{QQC}, 10^{-36} esu	$\delta_{NLR}/\gamma_{QQC}$, 10^{36} RGM/esu	γ_E/γ_{QCC}
0.0201±0.0014	0.294±0.021	2.4	0.1226±0.0085	0.80±0.06
2.49±0.22	84.9±7.5	292.73	0.290±0.026	2.67±0.24
0.86±0.29	25.9±8.7	57.17	0.45±0.15	2.9±1.0
-5.94±0.36	-293±18	726.34	0.404±0.024	3.72±0.22
-13.5±2.0	-920±140	1701.67	0.544±0.080	5.00±0.74
-21.2±2.8	-1860±250	2562.50	0.726±0.095	6.67±0.88
-4.93±0.66	-277±37	765.66	0.362±0.048	3.34±0.44
-6.7±1.0	-271±41	346.18	0.78±0.12	5.11±0.76
-2.61±0.36	-123±17	387.31	0.319±0.044	3.59±0.50
27.5±3.4	840±110	136.93	6.18±0.76	–
3.39±0.43	135±21	466.82	0.289±0.045	2.68±0.41
-1.05±0.11	-109±11	–	–	–
2.52±0.62	96±24	–	–	–
2.20±0.54	80±20	–	–	–
1.119±0.095	52.5±4.5	520	0.1009±0.0085	4.25±0.36
1.97±0.30	104±16	1040	0.099±0.015	3.53±0.54
2.13±0.21	91.5±9.0	980	0.0934±0.0092	4.08±0.40
1.34±0.18	67.8±9.1	460	0.147±0.020	4.4±0.59
1.06±0.23	39.8±8.6	109	0.365±0.079	3.43±0.74
2.49±0.35	102±14	203	0.503±0.071	4.73±0.66
-18.7±2.2	-920±110	547	1.68±0.20	–
-19.3±2.0	-1200±120	1084	1.11±0.11	–
-19.5±2.3	-2090±250	1973.22	1.06±0.12	14.6±1.7
-4.41±0.51	-940±110	1843.47	0.510±0.059	7.09±0.82
19.47±0.73	4380±1600	2507.21	1.75±0.065	24.30±0.91
-8.4±1.1	-1980±260	2998.73	0.659±0.086	9.12±1.2
12.5±1.9	2140±320	1626.06	1.31±0.20	18.2±2.7
-5.4±1.4	990±260	1814.43	0.54±0.14	7.5±1.9

3.3. Experimental value comparison to Quantum Chemical calculations

Experimental and QCC value comparison was done in two ways:

- From linear polarizability values acquired with the QCC molecular reorientation contribution was acquired and compared with experimental results,
- Experimental values of the Kerr coefficient were converted to second-order hyperpolarizability and compared to the QCC results.

Linear polarizability. First, let's consider chloroform. QCC gave the fallowing linear polarizability values for chloroform - $\alpha_{xx}=\alpha_{yy}=56$ Bohr^3, $\alpha_{zz}=29$ Bohr^3. By using equation (1.12) molecular reorientation contribution was calculated to be $n_2=2.0\cdot10^{-15}$ cm^2/W which is close to the experimental value. As polarization-resolved measurements showed that for pure chloroform refractive index changes are mainly due to reorientation, this was expected and confirms the QCC precision for the case of chloroform. For DMABI linear polarizability had a different value in each of the directions for which QCC gave the following values - $\alpha_{xx}=609$ Bohr^3, $\alpha_{yy}=277$ Bohr^3, and $\alpha_{zz}=111$ Bohr^3. Gaussian 09 gives values in CGS system and converts linear polarizability from cm^3 to Bohr^3 where Bohr stands for the Bohr radius with 1 Bohr = $5.29\cdot10^{-9}$ cm. Molecular reorientation contribution was calculated to be $n_2=2.0\cdot10^{-13}$ cm^2/W. After separating both components of electronic and molecular reorientation response by polarisation dependent measurement, the experimental value for molecular reorientation contribution to refractive index changes at 30 ps scale was $n_2=(1.5\pm0.1)\cdot10^{-13}$ cm^2/W. This value is smaller than the QCC result. This could be due to two factors: i) QCC is not able to precisely calculate linear polarizability; ii) Molecular reorientation effect has a longer time constant than 30 ps and has not reached an equilibrium state.

Second-order hyperpolarizability. Results for selected molecules second-order hyperpolarizability, nonlinear refractive cross-section, 2PA cross-section, and the ratio of the nonlinear refractive cross-section to second-order hyperpolarizability are presented in Table 3.2. By looking at ratio value $\delta_{NLR}/\gamma_{QQC}$ the value various quite a lot from 0.12 to 1.74 with the special exception of DMABI-OH of 6.18. One of the reasons for this large divergence from general values could be due to photochemical processes present during measurement. One of the explanations could be that the –OH group can be easily ionized with laser irradiation by removing a proton.

To better understand these results we will look in more detail of the ratio between experimental and QCC values for second-order hyperpolarizability. Firstly let's consider pure chloroform and DMABI. In Table 3.3 values for experimental,

QCC, and QCC values converted from convention IV (calculation value system) to I (experimental value system) of second-order hyperpolarizability are shown.

Table. 3.3: *Second-order hyperpolarizability of chloroform and DMABI. Values VI (definition used in calculations) and I (experimental definition) corresponds to different definitions of second-order hyperpolarizability*

Compound	γ_E, esu · 10^{-36}	$\gamma_{A,IV}$, esu · 10^{-36}	$\gamma_{A,I}$, esu · 10^{-36}
Chloroform	1.92±0.10	2.45	0.41
DMABI	3.07±0.69	2.97	0.495

Other literature works that have measured the Kerr effect for chloroform in fs range to determine fast component gives values in the range from 0.52-0.89·10^{-34} esu indicating larger values than QCC values. This also is a bit contradictory to experimental results that gave mainly reorientation contribution to refractive index changes. One of the reasons could be as through this work, and also in literature, when describing experimental results – two assumptions are made:

1. The solution is an isotropic media that gives specific relation to effective third-order susceptibility,
2. The induced effect is instantaneous compared to the laser pulse duration.

Next, let's look at DMABI results in more detail. Nonlinear refractive index and second-order hyperpolarizability values for DMABI are shown in Table 3.3. For DMABI the second-order hyperpolarizability values are quite close to each other, but when changing the Convention the values are an order apart. Both chloroform and DMABI show that it is very complicated to straightforwardly analyze the ratio between experimental and calculation results and all further analysis will only be carried based on comparing different molecules to each other.

Now let's compare results for other organic components. Firstly comparison of second-order hyperpolarizability will be carried out for molecules that possessed no significant 2PA and one-photon absorption at half-wavelength and acquired value is closer to the non-resonant case. For these molecules, the ratio between experimental and QCC results is around 2.6–4.7 and seems indifferent to the absolute value of second-order hyperpolarizability (see Figure 3.13). This shows that QCC values for these molecules can be used to estimate which molecules will have a larger Kerr response as the ratio value is independent of the absolute value of second-order hyperpolarizability.

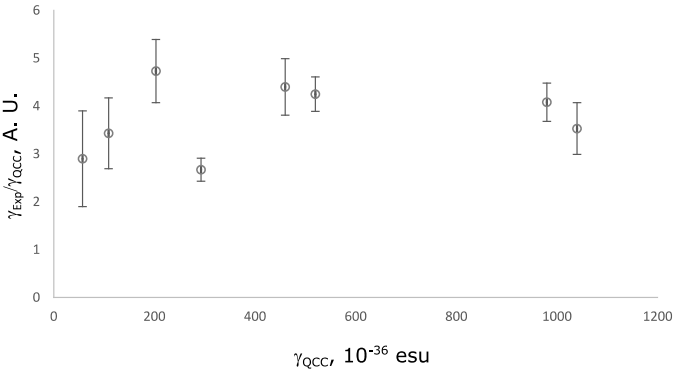

Figure. 3.13: *The ratio of experimental and QCC values of second-order hyperpolarizability as a function from QCC values.*

Next, let's consider molecules with 2PA effect and one-photon absorption at half-wavelength. In this case, a bigger focus will be given to the ratio between experimental and QCC results (ratio γ_E/γ_{QCC}) compared to 2PA cross-section values. This correlation is shown in Figure 3.14. Here TPA 7 and TPA 8 are excluded due to not fitting the linear trend and possessing much higher ratio values. This could be due to aggregation effects as they can lead to an increase in the Kerr effect. Previously in the literature, there have been observations that aggregation can lead to an increase in Kerr effect around 2 to 3 times[42] that correlates with over observed results. From this graph it is evident that for molecules with a strong 2PA correlation between ratio γ_E/γ_{QCC} values and 2PA cross-section values is observed.

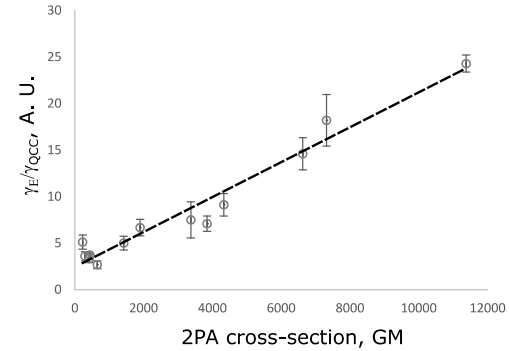

Figure 3.14: *Ratio of experimental and QCC values of second-order hyperpolarizability as function from Two-photon cross-section values.*

Comparing both molecule groups a distinctive difference can be observed:

- Molecules that do not possess any 2PA at irradiation wavelength and linear absorption at half-wavelength have a linear correlation between

QCC values and experimental values, indicated by a ratio of both values around 3.6±1,

- Molecules that possess 2PA irradiation wavelength and/or linear absorption at half-wavelength have a linear correlation between the ratio of experimental to QCC values and 2PA cross-section.

These conclusions can be used to further tune QCC methods to better predict experimental results and step towards material screening through QCC. It is important to again stress that here experimental value consists of both molecular reorientation and electronic contributions. For some compounds, molecular reorientation was evaluated through QCC results of linear polarizability. The results for these molecules are shown in Table 3.4. While the molecular reorientation contribution is quite significant for molecules with small Kerr values (ABI compounds excluding DiDMABI and TriDMABI), it becomes insignificant for larger ones. When comparing how average γ_E/γ_{QCC} ratio value and its error for molecules with small Kerr values changes when molecular reorientation is taken into account a shift from 4.52±1.3 to 5.7±1.0 can be observed. It is important to emphasize that these number do not correspond to previously mentioned ratio value for molecules with no significant 2FA as molecule selection differed. In general this is only significant for lower values and does not explain the overall linear trend observed in Figure 3.17.

Table 3.4: *QCC results for molecular reorientation contribution to refractive index changes*

Molecule	$n_{2;QCC/MR}$, $cm^2/W \cdot 10^{-12}$	$n_{2;Exp}$, $cm^2/W \cdot 10^{-12}$	$n_{2;QCC/MR}/n_{2;Exp}$
DMABI-Ju	0.191	-0.67±0.10	0.29
DMABI-dPh	0.154	-0.594±0.036	0.26
DiDMABI	0.21	-1.35±0.20	0.15
TriDMABI	0.17	-2.12±0.28	0.08
DDMABI	0.254	0.339±0.043	0.75
tB-DMABI-Ju	0.169	-0.261±0.036	0.34
tB-DMABI-dPh	0.143	-0.493±0.066	0.55

Conclusions

Here the main conclusions of this work are presented. Conclusions will be divided into three parts – NLO measurement methods, NLO properties of organic materials, and experimental result comparison to QCC.

Methods: Regarding third-order NLO measurement methods two different methods were tested in this work – the Z-scan and the MZI. Both methods were tested with 8 ns and 30 ps 1064 nm lasers. By comparing both methods the following conclusions were made:

- *Z-scan* – a good general method for NLO measurements. The main limitation of the Z-scan method is measuring samples with large induced phase changes due to complicated analytical models. This is not an issue for general material studies as often low concentration samples are studied with weak NLO signals.
- *MZI* – the main advantage of MZI is the simple analytical model for data fitting that can be used for small or large phase changes (around 3π). For phase changes larger than 3π the beam size variation starts to influence results. Also, MZI is hard to implement experimentally when short pulse lasers (ps scale) are used. Due to this, MZI is not the best method for Kerr effect studies where short pulse lasers are preferred but has its applicability in ns region measurements in the case when large phase change takes place, for example, photoisomerization in thin-films[43].

A more in-depth study of the Z-scan method was carried out to give general guidelines for correct Kerr effect evaluation with the main focus on separating molecular reorientation contribution from the electronic response of organic compounds when they are dissolved in chloroform. The main conclusions from this section were:

- In general ns laser pulse width should not be long enough to induce a thermal response from liquids with no significant linear absorption or 2PA at irradiation wavelength. But at higher pulse repetition rates this can happen due to accumulative thermo-optical effect and can overwhelm the Kerr effect. This holds up for pure organic solvents as well as for organic dyes dissolved in solvents. To be sure whether measured refractive index changes of organic dyes are due to Kerr or thermo-optical effect, polarisation dependent Z-scan measurements need to be implemented, especially for ns or longer pulse lasers,
- Polarisation resolved Z-scan measurements can be used to determine the ratio of molecular and electronic contributions to the Kerr effect.

This is a simpler approach than measuring the Kerr effect at different pulse widths. While electronic response can be separated this way, a more complicated aspect is the separation of the molecular response into libration and diffusive reorientation components and would demand pulse width dependent measurements to do this correctly.

Materials: Next a brief overview of conclusions from organic material measurements will be given.

- ABI derivatives: i) A correlation between linear absorption and 2PA cross-section was observed, indicating that the virtual state for 2PA transition and first excited state could be located close to each other; ii) 2PA effect increases when using lasers with longer pulse widths and scales proportionally to pulse width. A similar effect was observed for the Kerr effect in the case of DMABI that could be due to two-photon contribution to the Kerr effect increasing; iii) By increasing the ABI branch number attached to the TPA group 2PA effect increased linearly while the Kerr effect increased quadratically. This is because both dipolar and the two-photon contributions of the Kerr effect increased with the number of ABI groups.
- TPA derivatives – The angle between methyl or methoxy groups to the central NC_3 group significantly influences the Kerr coefficient value. A smaller angle leads to a larger Kerr effect.
- BIT derivatives – These materials have large 2PA cross-sections indicating that they could be applicable for optical limiting in the infra-red region.

Experiment vs QCC: From the comparison of experimental values to QCC the main conclusions regarding organic materials were:

- Molecules that do not possess any 2PA at irradiation wavelength and linear absorption at half-wavelength have a linear correlation between scaling factor between experimental/QCC values and QQC values, indicated by a ratio of both values around 3.6±1.0.
- For molecules that possess 2PA effect irradiation wavelength and/or linear absorption at half-wavelength scaling factor grows 2PA cross-section.
- Also, QCC results for molecular reorientation show, that this contribution is significant only for a molecule with small Kerr values ($\approx 2 \cdot 10^{-13}$ cm^2/W).

Thesis

- Separation of Kerr and thermo-optical contributions to refractive index changes by the Z-scan method can be done by polarisation and pulse repetition rate-dependent measurements. This can allow studying the Kerr effect using up to ns pulse width lasers.

- To correctly separate the electronic and the molecular contributions to the Kerr coefficient for organic chromophores dissolved in solvents polarization-resolved measurements must be used.

- When using Quantum Chemical calculations for predicting Kerr effect values for organic chromophores, molecular reorientation contribution can be calculated accurately from values of linear polarizability while a significant error for electronic contribution arises due to disregard of two-photon contribution.

References

1. Samoc, M. *et al. Journal of the Optical Society of America B,* **15**, 817 (1998).
2. Sheik-Bahae, M. *et al. IEEE J. Quantum Electron.* **26**, 760–769 (1990).
3. Melhado, M. S. *et al. Optics Express,* **28**, 3352 (2020).
4. Nitiss, E. *et al. Physica status solidi (a) applications and materials science,* **212**, 1867–1879 (2015).
5. Miller, R. C. *Applied Physics Letters,* **5**, 17–19 (1964).
6. Mizrahi, V. *et al. Physical Review Letters,* **55**, 696–699 (1985).
7. Wynne, J. J. *Physical Review,* **178**, 1295–1303 (1969).
8. Wynne, J. J. *et al. Applied Physics Letters,* **12**, 191–192 (1968).
9. Rustagi, K. C. *et al. Optics Communications,* **10**, 258–261 (1974).
10. Hermann, J. P. *et al. Applied Physics Letters,* **23**, 178–180 (1973).
11. Hermann, J. P. *et al. Journal of Applied Physics,* **45**, 5100–5102 (1974).
12. Gorman, C. B. *et al. Proceedings of the National Academy of Sciences of the United States of America,* **90**, 11297–11301 (1993).
13. Zojer, E. *Journal of Chemical Physics,* **116**, 3646 (2002).
14. Webster, S. *et al. Chemical Physics,* **348**, 143–151 (2008).
15. Fu, J. *et al.* J*ournal of the Optical Society of America B,* **24**, 67 (2007).
16. Padilha, L. A. *et al. Journal of Materials Chemistry,* **19**, 7503 (2009).
17. Karna, S. P. *et al. ACS Symposium Series*, **1**, 1–22 (1996).
18. Kuzyk, M. G. *et al. Advances in Optics and Photonics,* **5**, 4 (2013).
19. Stegeman, G. *et al. Optics Express,* **19**, 22486 (2011).
20. Meyers, F. *et al. Journal of the American Chemical Society,* **116**, 10703–10714 (1994).
21. del Coso, R. *et al. Journal of the Optical Society of America B* **21**, 640 (2004).
22. Ferdinandus, M. R. *et al. Optical Materials Express,* **2**, 1776 (2012).
23. Boyd, R. W. *Elsevier/Academic Press*, 2008
24. Reichert, M. *et al. Optica,* **1**, 436 (2014).
25. Bucaro, J. A. *et al. Journal of Chemical Physics,* **54**, 3846–3853 (1971).
26. Cubeddu, R. *et al. Physical Review A,* **2**, 1955–1963 (1970).
27. Close, D. H. *et al. IEEE Journal of Quantum Electronics,* **2**, 553–557 (1966).
28. Bishop, D. M. *et al. Journal of Chemical Physics,* **108**, 10013–10017 (1998).
29. Udayakumar, D. *et al. Chemical Physics,* **331**, 125–130 (2006).
30. Tutt, L. W. *et al. Progress in Quantum Electronics*, **17**, 299–338 (1993).
31. Shetty, T. C. S. *et al. Materials Technology*, **32**, 140–147 (2017).
32. Quan, C. *et al. Applied Surface Science,* **457**, 115–120 (2018).

33. Saad, N. A. *et al. Journal of Materials Science,* **54**, 188–199 (2019).
34. Chapple, P. B. *et al. Journal of Nonlinear Optical Physics & Materials,* **06**, 251–293 (1997).
35. Liu, Z.-B. *et al. Optics Express* **15**, 13351 (2007).
36. Yan, X.-Q. *et al. Optics Express* **17**, 6397 (2009).
37. Ganeev, R. A. *et al. Applied Physics B,* **78**, 433–438 (2004).
38. Zhao, P. *et al. Optica* **5**, 583 (2018).
39. Samoc, A. *Journal of Applied Physics,* **94**, 6167–6174 (2003).
40. Cabrera *et al. Condensed Matter Physics.* **9**, 385 (2006).
41. Liang, J. *et al. Journal of Applied Physics,* **101**, 013106 (2007).
42. Breukers, R. D. *et al. Optical Processes in Organic Materials and Nanostructures II*, **8827**, 88270N (2013).
43. Yang, L. *et al. Dyes and Pigments* **102**, 251–256 (2014).

Authors list of publications

Incorporated in this work:

1. **A. Bundulis**, E. Nitiss, I. Mihailovs, J. Busenbergs, M. Rutkis, *Study of Structure–Third-Order Susceptibility Relation of Indandione Derivatives*, The Journal of Physical Chemistry C, **120**, 27515–27522, 2016.
2. D. Gudeika, **A. Bundulis**, I. Mihailovs, D. Volyniuk, M. Rutkis, J. V. Grazulevicius, *Donor and acceptor substituted triphenylamines exhibiting bipolar charge-transporting and NLO properties,* Dyes and Pigments, **140**, 431–440, 2017.
3. **A. Bundulis**, I. Mihailovs, E. Nitiss, J. Busenbergs, M. Rutkis, *Determination of Kerr and two-photon absorption coefficients of indandione derivatives*, Proceedings SPIE, Nonlinear Optics and Applications, **10228**, 1022804, 2017.
4. **A. Bundulis**, E. Nitiss, J. Busenbergs, M. Rutkis, *Mach–Zehnder interferometer implementation for thermo-optical and Kerr effect study*, Applied Physics B, **124**, 56, 2018.
5. **A. Bundulis**, E. Nitiss, M. Rutkis, *Determination of Kerr and two-photon absorption coefficients of ABI thin films*, Proceedings SPIE, Nonlinear Optics and Applications, **10684**, 1068426, 2018.
6. **A. Bundulis**, M. Rutkis, *Determination of Third-order Nonlinear Optical Properties of ABI Derivatives*, Sensors & Transducers Journal, **233**, 46–50, 2019.
7. D. Gudeika, **A. Bundulis**, S. Benhattab, M. Ben Manaa, N. Berton, J. Bouclé, F. Tran Van, B. Schmaltz, D. Volyniuk, M. Rutkis, J. V. Grazulevicius, *Multifunctional derivatives of dimethoxy-substituted triphenylamine containing different acceptor moieties*, SN Applied Sciences, **2,** 327, 2020.
8. **A. Bundulis**, I. Mihailovs, M. Rutkis, *Origin of the Kerr effect: investigation of solutions by polarization-dependent Z-scan*, Journal of the Optical Society of America B, **37**, 1806–1811, 2020.

Other publications:

- E. Nitiss, **A. Bundulis**, A. Tokmakov, J. Busenbergs, E. Linina, M. Rutkis, *Review and comparison of experimental techniques used for determination of thin film electro-optic coefficients*, Physica Status Solidi (A) Applications and Materials Science, **212**, 1867–1879, 2015.

- E. Linina, **A. Bundulis**, E. Nitiss, M. Rutkis*, Poling dynamics of an EO active material using parallel-plate electrodes,* Proceedings SPIE, Nonlinear Optics and Applications, **10228**, 1022816 2017.
- K. Traskovskis, **A. Bundulis**, I. Mihailovs, *Unusual response to environmental polarity in a nonlinear-optical benzylidene-type chromophore containing a 1,3-bis(dicyanomethylidene)indane acceptor fragment*, Physical Chemistry Chemical Physics, **20**, 404–413, 2018.
- E. Nitiss, **A. Bundulis**, A. Tokmakov, J. Busenbergs, M. Rutkis, All-*Organic Waveguide Sensor for Volatile Solvent Sensing*, **9**, 356–366 Photonic Sensors, 2019.

Thesis in Conferences

1) **A. Bundulis**, E. Nitiss, J. Busenbergs, M. Rutkis, ISSP 32nd Scientific Conference, Riga, Latvia, February 17–19, 2016, page 31.
2) **A. Bundulis**, E. Nitiss, J. Busenbergs, M. Rutkis, DOC 2014, Riga, Latvia, April 9–12, page 27.
3) **A. Bundulis**, E. Nitiss, J. Busenbergs, M. Rutkis, DOC 2016, Riga, Latvia, March 21–23, page 10.
4) **A. Bundulis**, E. Nitiss, M. Rutkis, ISSP 33rd Scientific Conference, Riga, Latvia, February 22–24, 2017, page 6.
5) **A. Bundulis**, E. Nitiss, M. Rutkis, DOC 2017, Riga, Latvia, April 6–7, page 7.
6) **A. Bundulis**, E. Nitiss, M. Rutkis, I. Mihailovs, SPIE Optics + Optoelectronics, Prague, Czech Republic, April 24–27, 2017, page 15.
7) **A. Bundulis**, E. Nitiss, M. Rutkis, DOC 2018, Riga, Latvia, April 12–13, page 40.
8) **A. Bundulis**, E. Nitiss, M. Rutkis, I. Mihailovs, SPIE Photonics Europe, Strasbourg, France, April 22–26, 2018, page 123.
9) **A. Bundulis**, 10th Optoelectronics and Photonics winter school, Andalo, Italy, January 20–26, 2019.
10) **A. Bundulis,** M. Rutkis, 2nd International Conference on Optics, Photonics and Lasers (OPAL' 2019), Amsterdam, The Netherlands, April 24–26, 2019, Conference Proceeding p. 34–35.
11) **A. Bundulis**, M. Rutkis, ISSP 36th Scientific Conference, Riga, Latvia, February 11–13, 2020, page 25.

Acknowledgments

I would like to thank my supervisor Martins Rutkis for his consultations and guidance during these four years of making this work. Also, thank Igors Mihailovs for help with Quantum Chemical calculations and advice on result interpretation as well as Janis Busenbergs for help with the creation of electronic components for experimental setups. I would also like to express my special thanks to Edgars Nitiss for the support, advice and guidance in science that helped to overcome many challenges during this work.

I want to thank all the colleagues from the Laboratory of Organic Materials for advice and inspiration when it was most needed.

I would like to thank ISSP for the possibility to carry my work here as well as colleagues from RTU for synthesizing novel organic materials studied in this work.

Finally, I would like to thank everyone else who helped in the process of making this work.

This work could not be carried out without financial support from the following projects:

- Scientific Research Project for Students and Young Researchers Nr. SJZ2015/16 realized at the Institute of Solid State Physics, University of Latvia,
- The National Research program IMIS2 project “Photonics and Materials for Photonics”,
- Scientific Research Project for Students and Young Researchers Nr. SJZ/2016/10 realized at the Institute of Solid State Physics, University of Latvia
- ERDF 1.1.1.1 activity project Nr. 1.1.1.1/16/A/046 “Application assessment of novel organic materials by prototyping of photonic devices".